

## CALORIMETRY OF ACTIVE GALACTIC NUCLEUS JETS: TESTING PLASMA COMPOSITION IN CYGNUS A

M.KINO<sup>1</sup>, N.KAWAKATU<sup>2</sup>, AND F.TAKAHARA<sup>3</sup>

*Draft version July 5, 2021*

### ABSTRACT

We examine plasma composition of jets in active galactic nuclei through the comparison of the total pressure ( $P$ ) with partial pressures of electrons and protons in a cocoon. The total pressure is estimated from the analysis of an expanding cocoon dynamics. We determine the average kinetic energy per particle for several representative cases of particle energy distribution such as one- and two-temperature thermal plasmas and non-thermal electrons by evaluating the dissipation of total kinetic energy of the jet into the internal energy of cocoon plasma. The number density of the total electrons/positrons ( $n_{\pm}$ ) in the cocoon is constrained by using the particle supply from hot spots and the absence of thermal bremsstrahlung emission from radio lobes. By inserting  $P$ ,  $n_{\pm}$  and the particle energy of each population into the equation of state, the number density ( $n_p$ ) and pressure ( $P_p$ ) of protons in the cocoon can be constrained. Applying this method to Cygnus A, we find that (i) electron/positron ( $e^{\pm}$ ) pairs always dominate in terms of number density, but that (ii) either an “ $e^{\pm}$ -supported cocoon (i.e.,  $P_{\pm} > P_p$ )” or “proton-supported one (i.e.,  $P_{\pm} < P_p$ )” is possible.

*Subject headings:* galaxies: individual(Cygnus A) — magnetic fields — radiation mechanisms: non-thermal — radio continuum: galaxies — X-ray: galaxies

### 1. INTRODUCTION

Elucidating the formation mechanism of relativistic jets in active galactic nuclei (AGNs) is one of the greatest challenges of astrophysics in this century (e.g., Blandford and Znajek 1977; McKinney 2006; Komissarov et al. 2007; McKinney et al. 2012). Plasma composition of jets is a fundamental but difficult issue (Begelman et al. 1984 for review), because emission timescales of the bulk population such as low-energy electrons/positrons and protons are too long. To examine plasma composition, discrete blobs in blazar jets have been utilized over the years. So far, three approaches have been pursued. The first is based on the synchrotron self-absorption limit combined with total kinetic powers of jets (Reynolds et al. 1996; Hirovani et al. 1999, 2000; Hirovani 2005). The literature indicates the existence of  $e^{\pm}$  pair plasma in M 87, 3C 279 and 3C 345. The second is the constraint by the detection of circular polarization. Wardle et al. (1998) and Homan et al. (2009) examined the case of 3C 279 and found that the minimum Lorentz factor of non-thermal electrons/positrons should be much larger than unity for electron-proton (hereafter  $e/p$ ) content. They rather favored an alternative possibility of dominant  $e^{\pm}$  pair content with a small minimum Lorentz factor of non-thermal electrons/positrons (see, however, Ruszkowski and Begelman 2002). The third approach is the constraint from the absence of bulk-Compton emission in flat spectrum radio quasars (Sikora and Madejski 2000; Ghisellini & Tavecchio 2010) and it has been observationally tested for PKS 1510-089 and SWIFT J0746.3+2548 (Kataoka et al. 2008; Watanabe et al. 2009). The same

approach has also been applied to the kiloparsec-scale knots in PKS 0637-752 (Georganopoulos et al. 2005; Uchiyama et al. 2005; Mehta et al. 2009). They claim that jets contain more  $e^+e^-$  pairs than protons, but that jets are dynamically dominated by protons. However, it should be noted that the estimate of a total kinetic power  $L_j$  of each blob is difficult, because of the existence of invisible components such as low-energy electrons/positrons and protons. Therefore, the assumption of constant  $L_j$  was made and the  $L_j$  are inferred from non-thermal emissions. Since plasma composition is sensitive to  $L_j$ , a better estimate of  $L_j$  is essential. Regarding to the estimate of  $L_j$ , it is essential to take into account of the thermal component (e.g., Kino and Takahara 2008).

Cocoons associated with Fanaroff-Riley I and II (FR I and FR II) radio galaxies are also known to be good tools for exploring plasma composition. In contrast to blobs in blazars, investigations using cocoon dynamics allow us to better estimate of energy injection into the cocoon. The total pressure  $P$  can be estimated with fewer uncertainties based on the dynamical interaction between jets and the intra-cluster medium (ICM) and  $P$  involves the contributions of invisible components (e.g., Rawlings and Sanders 1991; Fabian et al. 2002). For FR I radio galaxies, many authors have discussed the ratio of  $P$  to that of non-thermal electrons ( $P_{-}^{\text{NT}}$ ) for various sources based on observed non-thermal emissions (e.g., Dunn et al. 2005; Croston et al. 2005; Rafferty et al. 2006; De Young 2006; Bîrzan et al. 2008). First of all, we should emphasize that these studies indicate that the total pressure  $P$  tends to be larger than that of non-thermal electrons, i.e.,  $P > P_{-}^{\text{NT}}$  (e.g., Bîrzan et al. 2008). This means that the finite pressure of low-energy electrons/positrons and/or protons is required in these sources. The derived  $P/P_{-}^{\text{NT}}$  values in the previous work extend over a wide range from the order of unity to thousands (e.g., Bîrzan et al. 2008; Cavagnolo et al. 2010). For FR I sources,

<sup>1</sup> National Astronomical Observatory of Japan 2-21-1 Osawa, Mitaka, Tokyo, 181-8588, Japan

<sup>2</sup> Graduate School of Pure and Applied Sciences, University of Tsukuba, 305-8571 Tsukuba, Japan

<sup>3</sup> Department of Earth and Space Science, Osaka University, 560-0043 Toyonaka, Japan

however, an entrainment process of surrounding medium via the jet boundary layer could work (e.g., De Young 1993; Bicknell 1984; Rossi et al. 2008) and the process makes jets heavier. Therefore, jets in FR I sources could undergo severe proton loading during their propagations and this could cause the large scatter of  $P/P^{\text{NT}}$ .

Instead, in this work, we focus on FR II radio galaxies (Fig. 1) from the viewpoint of the important advantage they represent. Contrary to FR I sources, we know from relativistic hydrodynamic simulations that no significant entrainment appears for FR II sources (Scheck et al. 2002; Mizuta et al. 2004). Therefore, a plasma composition test for FR II radio galaxies would allow us to give better constraints on plasma composition in AGN jets without an entrainment effect. Regarding an observational indication of a difference between total and non-thermal pressures in FR II radio galaxies, Ito et al. (2008) (hereafter I08) recently examined for the following sources (Cygnus A, 3C 223, 3C 284 and 3C 219). In I08, they show that the energy density of total plasma is larger than the energy density of non-thermal electrons by the factor of 4-310 in the case of minimum-energy condition (e.g., Miley 1980; Kellermann and Pauliny-Toth 1981). This implies that the minimum-energy condition is violated, particle energy is dominant, and low-energy electrons/positrons and/or protons (i.e., cosmic-rays) are required to explain the total  $P$  in these FR II sources.

In §2, we describe the basic idea and assumptions of our method. In §3, we briefly explain the dynamical determination of the total pressure in the cocoon. In §4 we express  $P$  as functions of the number density ratio of protons to electrons. In §5, we explain details of the plasma composition test. It is applied to Cygnus A in §6. Summary and discussions are given in §7.

## 2. METHOD AND PROBLEM SETTING

Here, we describe the basic idea and assumptions of our method. In this work, the number densities of protons ( $n_p$ ), positrons ( $n_+$ ) and electrons ( $n_-$ ) are related using the parameter  $\eta$  as follows:

$$\begin{aligned} n_p &\equiv \eta n_- \\ n_+ &= (1 - \eta)n_- \quad (0 \leq \eta \leq 1), \end{aligned} \quad (1)$$

where the latter relation is derived from the charge neutrality condition. The case of  $\eta = 0$  corresponds to pure  $e^\pm$  plasma while  $\eta = 1$  corresponds to the pure  $e/p$  plasma. We denote that  $n_p = n_p^{\text{T}} + n_p^{\text{NT}}$ ,  $n_- = n_-^{\text{T}} + n_-^{\text{NT}}$ ,  $n_+ = n_+^{\text{T}} + n_+^{\text{NT}}$ , and  $n_\pm = n_- + n_+$  where  $n_\pm$  is the sum of the total number densities of electrons and positrons. Hereafter, superscripts T and NT represent thermal and non-thermal components, respectively. The distinction between thermal and non-thermal particles may not be trivial for relativistic plasmas. In this paper, we refer the thermal component to Maxwellian-like distribution characterized by the temperature, while we refer the non-thermal one to particles following a power-law distribution characterized by the power-law index and minimum and maximum energies as detailed below. Since we focus on relativistic plasmas in the present work, thermal component correspondingly has a relativistic temperature. Hence one should be cautious since most of observational papers refer the thermal component to non-relativistic plasmas (e.g., Garrington and Conway 1991).

The allocation of partial pressure of each plasma population is the central concern of this paper. In general,  $P$  is decomposed to

$$\begin{aligned} P &= P_- + P_+ + P_p + P_B \\ &= P_-^{\text{T}} + P_+^{\text{T}} + P_-^{\text{NT}} + P_+^{\text{NT}} + P_p^{\text{T}} + P_p^{\text{NT}} + P_B, \end{aligned} \quad (2)$$

where  $P_-^{\text{T}}$ ,  $P_+^{\text{T}}$ ,  $P_p^{\text{T}}$ ,  $P_-^{\text{NT}}$ ,  $P_+^{\text{NT}}$ ,  $P_p^{\text{NT}}$ , and  $P_B$  are, the partial pressures of thermal (T) electrons, thermal positrons, thermal protons, non-thermal (NT) electrons, non-thermal positrons, non-thermal protons, and a magnetic pressure respectively. We also define  $P_\pm = P_- + P_+$  as the sum of the total pressures of electrons and positrons. Throughout this work, we do not include the magnetic pressure because it is sub-dominant in  $P$ . Isobe et al. (2005) summarize the energy density of energetic electrons as typically being 10 times larger than that of magnetic fields in various radio lobes (e.g., Isobe et al. 2002; Tashiro et al. 1998, 2009; Hardcastle and Croston 2010) and it also holds in Cygnus A (Yaji et al. 2010).

### 2.1. Basic idea of the method

The essence of our method is as follows. First, the total pressure in the cocoon ( $P$ ) is determined through dynamical considerations following I08 where they obtained  $P$  via the comparison of the expanding cocoon model with radio observations. Second, average energy per one particle in the cocoon is evaluated. It is essential that our formulation is based on the basic conservation laws of mass, momentum, and energy in the cocoon. Since it depends on coupling of protons to the electrons/positrons, we examine several representative cases with different equations of state. Third,  $n_-$  can be partially constrained by using the absence of thermal bremsstrahlung emission from the cocoon and the supply rate of electrons from the hot spots. Finally,  $n_p$  and  $P_p$  can be obtained by inserting the obtained quantities into the equation of state (EOS).

### 2.2. On particle distribution functions

Since observational data at low frequencies below GHz are quite limited, it is hard to explore the properties of low-energy electrons (including positrons). Bearing this difficulty in mind, we pick up plausible cases of electron distribution function. As the canonical case referred to as case (a), we consider two-temperature thermal plasmas, where protons and electrons have different temperatures and contributions of non-thermal components to the total pressure are negligible. As an alternative, we also examine case (b) where protons and electrons take the same temperature without non-thermal components.

We further explore two cases (c) and (d) in which non-thermal population makes a dominant contribution to the total pressure with a negligible pressure of thermal population. For the non-thermal population, we assume the power-law distribution functions:

$$\begin{aligned} n_-^{\text{NT}}(\gamma_-) &\propto \gamma_-^{-s_e} (\gamma_{-, \text{min}} \leq \gamma_- \leq \gamma_{-, \text{max}}), \\ n_p^{\text{NT}}(\gamma_p) &\propto \gamma_p^{-s_p} (\gamma_{p, \text{min}} \leq \gamma_p \leq \gamma_{p, \text{max}}), \end{aligned} \quad (3)$$

for case (c) with  $s_p = s_e > 2$ . Observations of the spectral index in the radio lobe of Cygnus A suggest  $s_e > 2$  (e.g., Carilli et al. 1991; Yaji et al. 2010).

Lastly, we set case (d) in which the number spectrum of non-thermal electrons is given by a broken power law:

$$n_-^{\text{NT}}(\gamma_-) \propto \begin{cases} \gamma_-^{-s_{e,1}} & (\gamma_{-, \text{min}} \leq \gamma_- \leq \gamma_{-, \text{crit}}), \\ \gamma_{-, \text{crit}}^{s_{e,2}-s_1} \gamma_-^{-s_{e,2}} & (\gamma_{-, \text{crit}} \leq \gamma_- \leq \gamma_{-, \text{max}}), \end{cases} \quad (4)$$

$$n_p^{\text{NT}}(\gamma_p) \propto \gamma_p^{-s_p} (\gamma_{p, \text{min}} \leq \gamma_p \leq \gamma_{p, \text{max}}),$$

where  $s_{e,1} < 2$  and  $s_p > 2$  are satisfied. This model is based on Stawarz et al. (2007) who suggest that observed spectra at the jet termination shock (hot spot) of FR II jets (Cygnus A) can be explained by the break at non-thermal electron energy (hereafter  $\gamma_{\pm, \text{crit}}$ ). This type of spectra may be due to the absorption of electromagnetic waves emitted at the harmonics of cyclotron frequency of cold protons, as discussed by Hoshino et al. (1992) and Amato and Arons (2006). Some observations for other FR II sources could also be compatible with this picture (e.g., Perlman et al. (2010) for 3C445.)

For cases (c) and (d), the minimum energy of non-thermal electrons/positrons ( $\gamma_{\pm, \text{min}} m_e c^2$ ) and protons ( $\gamma_{p, \text{min}} m_e c^2$ ) are generally assumed as

$$\gamma_{\pm, \text{min}} \approx \gamma_{p, \text{min}} \approx \Gamma_j, \quad (5)$$

which is expected when protons and electrons/positrons are separately heated and accelerated at termination shocks. On the other hand, the values of the maximum energy of non-thermal pairs ( $\gamma_{\pm, \text{max}} m_e c^2$ ) and protons ( $\gamma_{p, \text{max}} m_p c^2$ ) are largely uncertain. While  $\gamma_{\pm, \text{max}} m_e c^2$  may be significantly affected by radiative coolings,  $\gamma_{p, \text{max}} m_p c^2$  may reach the range of highest energy cosmic-rays (e.g., Takahara 1990; Rachen and Biermann 1993). It is reasonable to suppose that  $\gamma_{\pm, \text{max}} \gg \gamma_{\pm, \text{min}}$  and  $\gamma_{p, \text{max}} \gg \gamma_{p, \text{min}}$ .

### 3. TOTAL PRESSURE $P$

In this section, we briefly describe the basic idea of estimating the total pressure  $P$ . In Fig. 1 we show a cartoon of the interaction of the jet and ICM. Heating and acceleration processes work at hot spots and those particles are injected into cocoons. The cocoon model was proposed by Begelman and Cioffi (1989) in which the dissipated energy of jet bulk motion is the origin of the total pressure of cocoon and a cocoon of FR IIs is expected to be overpressured against ICM pressure ( $P_{\text{ICM}}$ ) with a significant sideways expansion. Therefore, the assumption of  $P = P_{\text{ICM}}$  is not valid. We have proposed the method of dynamical constraint on  $P$  by comparison of the cocoon model with the actually observed morphology of the cocoons (Kino and Kawakatu 2005; I08) and the method is applied to various radio lobes (e.g., Machalski et al. 2010). We use this model in the present work. The reliability of the expanding cocoon model is well examined in Kawakatu and Kino (2006). The results of relativistic hydrodynamical simulations of Scheck et al. (2002) and Perucho and Marti (2007) support the above analytic model. The mass and energy injections from the jet into the cocoon, which govern the cocoon pressure  $P$  and mass density  $\rho$  averaged by the source age ( $t_{\text{age}}$ ) are written as

$$\frac{\hat{\gamma}}{\hat{\gamma} - 1} \frac{PV}{t_{\text{age}}} = 2T_j^{01} A_j \equiv 2L_j, \quad T_j^{01} = \rho_j c^2 \Gamma_j^2 v_j, \quad (6)$$

$$\frac{\rho V}{t_{\text{age}}} = 2J_j A_j, \quad J_j = \rho_j \Gamma_j v_j, \quad (7)$$

where  $\hat{\gamma}$ ,  $V$ ,  $A_j$ ,  $T_j^{01}$ ,  $J_j$ ,  $\rho_j$ , and  $\Gamma_j$  are the adiabatic index of the plasma in the cocoon, the volume of the cocoon, the cross-sectional area, the total energy flux, and rest mass flux, rest mass density, and bulk Lorentz factor of the jet, respectively. The term  $V$  is evaluated as  $V = 2(\pi/3)\mathcal{R}^2 LS^3$ , where  $LS$  and  $\mathcal{R}$  are the linear size of the cocoon along the jet axis and the aspect ratio of the cocoon, respectively. Here we denote physical quantities of the jet with the subscript  $j$ . Throughout this work, we focus on a relativistic jet. Correspondingly, the shocked plasma has relativistic energy, thus we take  $\hat{\gamma} = 4/3$ . The  $PdV$  work done by the cocoon against ICM is taken into account in the energy equation Eq. (6) following I08. For given  $\rho_{\text{ICM}}$ , we can dynamically estimate total pressures  $P$  by measuring  $LS$ ,  $\mathcal{R}$ , and the head cross-sectional area of the cocoon. Here the relations of  $LS = \beta_{\text{hs}} c t_{\text{age}}$  and  $\mathcal{R} \equiv l_c / LS < 1$  hold where  $l_c$  and  $\beta_{\text{hs}} c$  are the lateral size of the cocoon and advance velocity of the hot spot, respectively. Since  $\mathcal{R}$  and  $\beta_{\text{hs}}$  have some uncertainties, actual  $P$  is bounded by maximum and minimum values

$$P_{\text{min}} \leq P \leq P_{\text{max}}. \quad (8)$$

Thus we can obtain the total pressure of cocoon  $P$ , which includes the partial pressures of non-radiating particles. The estimate of  $P$  has actually been done by I08 for some FR II sources and we adopt  $P$  values in I08 in this work.

### 4. PRESSURE AS A FUNCTION OF $\eta$

In this section, we express  $P$  as a sum of the partial pressures and represent it as a function of  $\eta$  (we call this Equation of State, EOS) for respective cases.

#### 4.1. Case (a)

First, we examine the canonical case of two-temperature thermal plasma. Here we assume that  $P_-^{\text{NT}} = P_+^{\text{NT}} = P_p^{\text{NT}} = 0$  and  $n_-^{\text{NT}} = n_+^{\text{NT}} = n_p^{\text{NT}} = 0$ . The EOS in the cocoon filled with relativistic plasma is given by

$$P \approx P_{\pm}^{\text{T}} + P_p^{\text{T}} \\ = (n_-^{\text{T}} + n_+^{\text{T}}) k T_{\pm} + n_p^{\text{T}} k T_p, \quad (9)$$

where  $T_{\pm}$ , and  $T_p$  are the electron/positron temperature, and proton temperature, respectively. Hereafter we adopt  $T_{\pm} = T_- = T_+$  where  $T_-$  and  $T_+$  are temperatures of electrons and positrons, respectively. Following Kino et al. (2007), we can obtain  $T_{\pm}$  and  $T_p$  from Eqs. (6), (7), and (9):

$$k T_{\pm} = \frac{\Gamma_j m_e c^2}{4}, \quad k T_p = \frac{\Gamma_j m_p c^2}{4}, \quad (10)$$

which are typically given by  $k T_{\pm} = 1.3 \left(\frac{\Gamma_j}{10}\right)$  MeV, and  $k T_p = 2.3 \left(\frac{\Gamma_j}{10}\right)$  GeV. Here we assume the limit of inefficient  $e/p$ -coupling i.e, protons and electrons are separately thermalized so that  $k T_{\pm} = (m_e/m_p) k T_p$  since plasma number densities in large scale jets are conservatively expected to be too dilute to achieve efficient  $e/p$ -coupling (e.g., Kino et al. 2007 and references therein).

The emission timescale is so long that radiative cooling is negligible. It is worth noting that the geometrical factors in Eqs. (6) and (7) are completely canceled out and  $kT_{\pm}$  and  $kT_p$  are governed only by  $\Gamma_j$ .

Inserting Eq. (10) into Eq. (9), we rewrite the total pressure in the cocoon  $P$  as

$$P(\eta) = 2.05 \times 10^{-6} n_{-}^{\text{T}} \left[ (2 - \eta) + \eta \frac{m_p}{m_e} \right] \left( \frac{\Gamma_j}{10} \right) \text{ erg cm}^{-3}, \quad (11)$$

where the first term and second term in the square bracket correspond to the partial pressure of pairs and protons, respectively.

#### 4.2. Case (b)

As an opposite extreme to case (a), here we consider the case of one-temperature plasma. In this example, some of the proton energy is somehow transferred to electrons/positrons to achieve an efficient  $e/p$ -coupling. Then hotter electrons/positrons and colder protons are produced. From the condition  $kT_{\pm} = kT_p$ , and Eqs. (6) and (7), we obtain

$$kT_{\pm} = kT_p = \frac{\Gamma_j m_e c^2}{8} \left[ (2 - \eta) + \eta \frac{m_p}{m_e} \right]. \quad (12)$$

In this case, each population (i.e.,  $p/e^-/e^+$ ) has the same kinetic energy. The total pressure is given by Eq. (11) the same as case (a). The essential difference from case (a) is that  $kT_{\pm}$  in case (b) is much higher than the one in case (a).

#### 4.3. Case (c)

For comparison with the canonical case (a), we examine case (c) when the cocoon pressure is dominated by non-thermal particles. Case (c) concerns when the spectral indices of non-thermal particle energy distributions satisfy  $s_p = s_e > 2$  as some theoretical work on relativistic shocks suggests (e.g., Bednarz and Ostrowski 1998; Kirk et al. 2000; Achterberg et al. 2001; Spitkovsky 2008; Sironi and Spitkovsky 2011) and as the radio lobes of Cygnus A show  $s_e > 2$  (e.g., Carilli et al. 1991; Yajima et al. 2010). In this case, electrons and protons with the lowest energies are the main carriers of energy. Then, the evaluation of partial pressures of non-thermal plasma is basically the same as in case (a) when we replace  $kT_{\pm}$  with  $\gamma_{\pm, \text{min}} m_e c^2$  and  $kT_p$  with  $\gamma_{p, \text{min}} m_p c^2$ . Then  $P$  is given by

$$P(\eta) = \frac{\Gamma_j n_{-}^{\text{NT}} m_e c^2}{3} \frac{s_e - 1}{s_e - 2} \left[ (2 - \eta) + \eta \frac{m_p}{m_e} \right]. \quad (13)$$

From this, it is clear that we can appropriately evaluate  $\eta$  for the case (c) by replacing  $n_{-}^{\text{T}}$  to  $n_{-}^{\text{NT}}$  in the same way as case (a).

#### 4.4. Case (d)

Here we examine the pressure of non-thermal electrons when they follow a broken power law spectrum Eq. (4). Stawarz et al. (2007) indicated  $\gamma_{\pm, \text{crit}} \sim m_p/m_e$  for the hot spots in Cygnus A. The energy of the electron component is governed by those with break energy, while the number is dominated by those with lowest energies.

Since  $s_p > 2$  is satisfied, lowest-energy protons carry the most energy. Therefore, the total pressure  $P$  is expressed as

$$P(\eta) = \frac{\Gamma_j n_{-}^{\text{NT}} m_e c^2}{3} \left[ \frac{s_{e,1} - 1}{-s_{e,1} + 2} A_{\pm} (2 - \eta) + \frac{s_p - 1}{s_p - 2} \eta \frac{m_p}{m_e} \right], \quad (14)$$

where  $A_{\pm} = (\gamma_{\pm, \text{crit}}/\gamma_{\pm, \text{min}})^{-s_{e,1}+2}$ . Thus  $\eta$  can be evaluated when we replace  $n_{-}^{\text{T}}$  to  $n_{-}^{\text{NT}}$  and include factor  $A_{\pm}$ .

### 5. TESTING PLASMA COMPOSITION

We explain the method for constraining plasma composition of AGN jets for thermal plasma cases (a) and (b) in 5.1, 5.2, and 5.3. The application to non-thermal plasma cases (c) and (d) can be readily understood and is explained in 5.4.

#### 5.1. Characteristic pressures

Firstly we define characteristic pressures which divide the number-density/pressure plane into several regions as shown in Fig. 2. As a preparation, here we define  $\eta_{\text{eq}}$

$$\eta_{\text{eq}} \equiv \frac{2}{m_p/m_e - 1} = 1.1 \times 10^{-3} \quad (P_{\pm} = P_p). \quad (15)$$

The partial pressure of proton-associated electrons is implicitly neglected since it is subdominant in the case of inefficient  $e/p$ -coupling. The line with  $n_{-} = 1 \times 10^3 n_p$  divides the pair-supported and proton-supported cocoon in the limit of inefficient  $e/p$ -coupling plasma. By definition, the cocoon with  $\eta > \eta_{\text{eq}}$  is proton-supported (dark gray region in Fig. 2) while the cocoon with  $\eta < \eta_{\text{eq}}$  is pair-supported one (light gray region in Fig. 2). When  $n_{-}$  is bounded by  $n_{-, \text{min}}$  and  $n_{-, \text{max}}$  as argued in the next subsection, the allowed region of  $n_{-}$  is segmented by some characteristic pressures by the characteristic values of  $n_{-}$  and  $\eta$ , i.e.,  $n_{-, \text{min}}$ ,  $n_{-, \text{max}}$ ,  $\eta = 0$ ,  $\eta = \eta_{\text{eq}}$ , and  $\eta = 1$ . Here, we define six characteristic pressures as follows;

$$\begin{aligned} P(\eta = 0; n_{-} = n_{-, \text{min}}) &\equiv P_{0, \text{min}}, \\ P(\eta = \eta_{\text{eq}}; n_{-} = n_{-, \text{min}}) &\equiv P_{\text{eq}, \text{min}}, \\ P(\eta = 0; n_{-} = n_{-, \text{max}}) &\equiv P_{0, \text{max}}, \\ P(\eta = \eta_{\text{eq}}; n_{-} = n_{-, \text{max}}) &\equiv P_{\text{eq}, \text{max}}, \\ P(\eta = 1; n_{-} = n_{-, \text{min}}) &\equiv P_{1, \text{min}}, \\ P(\eta = 1; n_{-} = n_{-, \text{max}}) &\equiv P_{1, \text{max}}. \end{aligned} \quad (16)$$

Then, by definition, we have the following relations

$$\begin{aligned} P_{0, \text{min}} : P_{\text{eq}, \text{min}} : P_{0, \text{max}} : P_{\text{eq}, \text{max}} : P_{1, \text{min}} : P_{1, \text{max}} \\ = 1 : 2 : \frac{n_{-, \text{max}}}{n_{-, \text{min}}} : 2 \frac{n_{-, \text{max}}}{n_{-, \text{min}}} : \frac{m_p}{m_e} : \frac{m_p}{m_e} \frac{n_{-, \text{max}}}{n_{-, \text{min}}}, \end{aligned} \quad (17)$$

where we approximate  $2 - \eta_{\text{eq}} \approx 2$ . To evaluate these pressures, we estimate  $n_{-, \text{min}}$  and  $n_{-, \text{max}}$  in the next subsection.

#### 5.2. Estimation of $n_{-}$

Here we constrain the number density of electrons in the cocoon ( $n_{-}$ ). We denote the lower and upper limits of  $n_{-}$  as  $n_{-, \text{min}}$  and  $n_{-, \text{max}}$ , respectively. The values of  $n_{-, \text{min}}$  and  $n_{-, \text{max}}$  are independently constrained and we show them below.

### 5.2.1. Lower limit of $n_-$

Here we estimate the lower limit of  $n_-$  and examine the case when the number density of thermal electrons is larger than that of non-thermal electrons  $n_-^T \geq n_-^{NT}$ , since non-thermal electrons are partially injected from the background thermal electrons. (Later, the extreme cases of  $n_-^T \leq n_-^{NT}$  will also be discussed, being identical to cases (c) and (d)). Since the shocked plasma at hot spots expands sideways and is injected into the cocoon, we can estimate  $n_-^{NT}$  by using  $n_{hs}^{NT}$  where  $n_{hs}^{NT}$  is the number density of non-thermal electrons in a hot spot. We stress that  $n_{hs}^{NT}$  is well constrained by observed non-thermal emissions of hot spots for FR II sources (e.g., Harris and Krawczynski 2006 for review). By connecting the number density from the jet to the cocoon based on Eq. (7) and shock conditions along the jet axis shown in Kino and Takahara (2004) (hereafter KT04), we obtain

$$n_{-,min} = \frac{n_{hs}^{NT} A_j L S}{2V\beta_{hs}}. \quad (18)$$

In general, number density of non-thermal electrons with power law distribution  $n_{hs}^{NT} \propto \int_{\gamma_{hs,min}}^{\gamma_{hs,max}} \gamma_{hs}^{-s_{hs}} d\gamma_{hs}$  can be given by

$$n_{hs}^{NT} \propto \gamma_{hs,min}^{-s_{hs}+1}. \quad (19)$$

We assume the standard value of  $s_{hs} \approx 2$  and  $\gamma_{hs,min} \approx \Gamma_j$ .

### 5.2.2. Upper limit of $n_-$

The upper limit of  $n_-$  can be constrained by the absence of thermal bremsstrahlung from hot electrons in the cocoon/lobes viewed in X-ray observations (Wilson et al. 2000, 2006). The observed X-ray emissions associated with radio lobes are non-thermal emissions and there is no evidence for thermal X-ray emission from cocoons/lobes (Harris and Krawczynski 2006 for review). From this, we can safely use the condition of  $L_{X,obs} > L_{brem}(n_-^T, T_{\pm})$  where  $L_{brem}/V = \alpha_f r_e^2 m_e c^3 (n_-^T)^2 F_{\pm}(\Theta_{\pm}) \text{ erg s}^{-1} \text{ cm}^{-3}$ ,  $F_{\pm}(\Theta_{\pm}) = 48\Theta_{\pm}(\ln 1.1\Theta_{\pm} + 5/4)$ , and  $\Theta_{\pm} = kT_{\pm}/m_e c^2$ , for bremsstrahlung at relativistic temperature (Eq. (22) in Svensson 1982) and  $\alpha_f$  and  $r_e$  are the fine structure constant and the classical electron radius, respectively. From this, we obtain the maximum  $n_-$  as follows:

$$n_{-,max} = \left( \frac{L_{brem}}{V\alpha_f r_e^2 m_e c^3 F_{\pm}(\Theta_{\pm})} \right)^{1/2}. \quad (20)$$

It is worth commenting on the availability of constraining the upper limit of  $n_-$  by the analysis of the internal depolarization of the radio lobes. Relativistic plasma makes a smaller contribution to Faraday rotations since electron inertia increases for the relativistic regime and it suppresses rotations of polarization angle (e.g., Ichimaru 1973; Melrose et al. 1997; Quataert and Gruzinov 2000; Huang and Shcherbakov 2011). Therefore, it is not effective to use the constraint by RM in the present work.

### 5.3. Estimation of $n_p$

Once  $n_-$  is estimated, the proton number density  $n_p$  can be determined as

$$n_p = \eta n_-, \quad (21)$$

by definition. Here, of course, the conditions of  $0 \leq \eta \leq 1$  and  $n_{-,min} \leq n_- \leq n_{-,max}$  are imposed. In Fig. 3, the allowed region of  $n_p$  is added to that of  $n_-$  shown in Fig. 2. In the same way as Fig. 2, the plane is divided into 5 regions.

Finally, the allowed regions of  $n_p$  and  $n_-$  can be obtained by adjoining the range of  $P$ . The allowed regions drawn in Fig. 3 are bounded by Eq. (8). Thus, we can obtain the definitive allowed regions of  $n_p$  and  $n_-$ .

### 5.4. Application to cases (c) and (d)

In 5.1, 5.2 and 5.3, we consider physical quantities associated with thermal plasma in cases (a) and (b). But those can also be applied to non-thermal plasma by the proper replacements of number densities and average energies of particles. With regard to average energies, we have already explained the replacements in the previous section. As for  $n_{-,min}$ , the estimate shown in 5.2.1. can be applied both for thermal and non-thermal plasma. As for  $n_{-,max}$ , the estimate shown in 5.2.2. can be applied only for thermal plasma. So, we do not use  $n_{-,max}$  for the cases (c) and (d). Thus we can properly estimate  $\eta$  for cases (c) and (d).

## 6. APPLICATION TO CYGNUS A

Here we apply the above method to Cygnus A ( $z = 0.0562$ ) which is one of the best studied FR II radio galaxies (e.g., Carilli and Barthel 1996; Steenbrugge et al. 2008, 2010; Yaji et al. 2010). The physical quantities of Cygnus A have been well constrained by previous work. To constrain the real values of  $P$  and  $n_-$ , we carefully evaluate  $\mathcal{R}$ ,  $\beta_{hs}$ , and  $\Gamma_j$ . The term  $\mathcal{R}$  has an effect on  $n_-$  via a cocoon volume  $V$ . The term  $\Gamma_j$  is directly proportional to  $P$ . The term  $\beta_{hs}$  controls the source age  $t_{age}$  which governs the injection rates of mass and energy into the cocoon. These are summarized in 6.1. The resultant allowed region of  $n_-$  and  $n_p$  is summarized in 6.2.

### 6.1. Viable ranges of physical quantities

We show adopted conditions of the model parameters for deriving the above results. We fix the cross section area of the jet as  $A_j = \pi R_{hs}^2 = \pi(2 \text{ kpc})^2$  (Wilson et al. 2000) and the number density of ICM just ahead of the hot spot as  $n_{ICM} = 0.5 \times 10^{-2} \text{ cm}^{-3}$  (the shell No. 6 in Table 5 in Smith et al. 2002).

- *Cocoon morphology  $\mathcal{R}$ .*

From images of the Cygnus A cocoon, we can directly constrain  $\mathcal{R}$ . The upper limit  $\mathcal{R} \approx 0.5$  is determined by the Chandra X-ray image (Wilson et al. 2000, 2006; Yaji et al. 2010). The lower limit  $\mathcal{R} \approx 0.25$  is directly measured by the 330 MHz VLA image (see also Carilli et al. 1991; Lazio et al. 2006). Therefore we set

$$0.25 \leq \mathcal{R} \leq 0.5,$$

in the present work.

- *Cocoon head velocity*  $\beta_{\text{hs}}$ .

Cocoon head velocity which equals the hot spot advance velocity ( $\beta_{\text{hs}}$ ) is well constrained by the synchrotron aging method. The estimated  $\beta_{\text{hs}}$  has some uncertainty due to the uncertainty of magnetic-field strength in the cocoon. From the result of synchrotron aging diagnosis in Carilli et al. (1991), we adopt the allowed range of  $\beta_{\text{hs}}$  as

$$0.01 \leq \beta_{\text{hs}} \leq 0.06.$$

We emphasize that sufficiently large uncertainty is taken into account here. The adopted value of  $\beta_{\text{hs}}$  is quite typical for hot spots in FR II radio galaxies (e. g., Scheuer 1995).

- *Lorentz factor of the jet*  $\Gamma_j$ .

It is difficult to determine the true velocity of the jet. At least we may say that apparent velocity of blobs obtained by VLBI observations show a minimum velocity of underlying flow. A fast apparent motion of a blob at the jet base ( $0.56 \pm 0.28$ )  $c$  has been reported by VLBI observations (Bach et al. 2003). Furthermore, suggestions of superluminal motion were made (Krichbaum et al. 1998; Bach et al. 2002) although they had not been clearly confirmed. On VLA scale, a clear asymmetry in brightness distribution of a kpc-scale jet due to a relativistic motion is seen (Perley et al. 1984). Therefore, overall radio observations seem to indicate relativistic motion. Bearing this in mind, we assume that the jet is relativistic and the four-velocity of the jet  $\Gamma_j\beta_j$  is set as

$$1 \leq \Gamma_j\beta_j \leq 30.$$

Here the upper limit is assumed as  $\Gamma_j \approx 30$  based on the statistical study of radio jets of MOJAVE sources (Lister et al. 2001, 2009; Kellermann et al. 2004).

- *Cocoon pressure*  $P$ .

Using the value of  $V = 1 \times 10^{70} \mathcal{R}^2 \text{ cm}^3$ , we can estimate the total pressure  $P$  as

$$8 \times 10^{-11} \text{ erg cm}^{-3} \leq P \leq 4 \times 10^{-9} \text{ erg cm}^{-3}. \quad (22)$$

The lower limit equals the ICM pressure  $8 \times 10^{-11} \text{ erg cm}^{-3}$  measured by Arnaud et al. (1984) to satisfy the over-pressured cocoon condition. Although the upper limit of  $P$  is basically adopted from I08, the value  $4 \times 10^{-9} \text{ erg cm}^{-3}$  is 4 times larger than the original estimate in I08. This is due to the change in minimum value of  $\mathcal{R}$  from 0.5 to 0.25 based on VLA's 0.3 GHz image. It should be stressed that our adoption of the allowed range of  $P$  is sufficiently wide compared with all of the previous work (e.g, Carilli 1998 for review). Note that Yaji et al. (2010) estimates that  $P_{-}^{\text{NT}}$  in the radio lobes as  $P_{-}^{\text{NT}} \approx (1 - 2) \times 10^{-9} \text{ erg cm}^{-3}$  for  $\gamma_{\pm} \approx 1$  which causes  $P_{-}^{\text{NT}} > P_{\text{min}}$ . So, if  $P$  completely equals the radio lobe pressure, then the range  $P_{\text{min}} \leq P < P_{-}^{\text{NT}}$  is excluded and the allowed  $P$  range becomes narrower. The allowed example with  $P_{\text{min}} \leq P_{-}^{\text{NT}} \leq P \leq P_{\text{max}}$  is involved in cases (c) and (d).

- *Non-thermal electron number density*  $n_{-, \text{hs}}^{\text{NT}}$ .

The lower limit  $n_{-, \text{min}}$  largely depends on  $n_{\text{hs}}^{\text{NT}}$ . For  $s_{\text{hs}} = 2$ , the number density of non-thermal electrons in the hot spot can be obtained from

$$n_{\text{hs}}^{\text{NT}} \approx 1 \times 10^{-3} \left( \frac{\gamma_{\text{hs}, \text{min}}}{10} \right)^{-1} \text{ cm}^{-3}, \quad (23)$$

via detailed comparisons of the SSC model with the observed broadband spectrum (Wilson et al. 2000; KT04; Stawarz et al. 2007) where  $\gamma_{\text{hs}, \text{min}} \approx \Gamma_j$ . We stress that these three independent papers derive similar values of  $n_{\text{hs}}^{\text{NT}}$  although Stawarz et al. (2007) adopts the different electron-distribution function shown in Eq. (4). Furthermore, we note the importance of low-frequency radio spectra since it affects the estimate of  $n_{\text{hs}}^{\text{NT}}$ . Regarding low-frequency radio observation, we briefly comment on the work of Lazio et al. (2006). They indicated spectral flattening and turnover at  $\sim 100$  MHz. However it seems difficult to determine these accurately because the spot sizes are smaller than the VLA beam sizes at the above frequencies. The LOw Frequency ARray (LOFAR) (<http://www.lofar.org/>) and Square Kilometer Array (SKA) (<http://www.skatelescope.org/>) will, in future, tell us the real turnover frequency with sufficiently high resolution.

- *Thermal electron number density*  $n_{-}^{\text{T}}$ .

Here we comment on the difficulty of constraining  $n_{-}^{\text{T}}$ . We use the absence of bremsstrahlung emission. The  $X$ -ray observations for Cygnus A show the flux upper limit as  $\sim 1 \times 10^{-13} \text{ erg s}^{-1} \text{ cm}^{-2}$  (e.g., Smith et al. 2002).

As already mentioned, the constraint from the intrinsic RM is not available, because plasma temperature is relativistic in the present work. Even worse, Cygnus A is known for its unusually large RM values and thus it is not a good example from which to argue the intrinsic depolarization (Dreher et al. 1987; Garrington and Conway 1991). No evidence for intrinsic depolarization between 5 and 15 GHz is found and the origin of the large RM is thought to be the external bow shock which surrounds the radio lobes (Dreher et al. 1987; Carilli et al. 1988). Hence it is not appropriate to use the constraint from RM for Cygnus A.

## 6.2. Results

Below we show resultant allowed region of  $n_{-}$  and  $n_p$  for cases (a), (b), (c) and (d).

### 6.2.1. Case (a)

Considering the uncertainties of  $\Gamma_j\beta_j$  and  $\beta_{\text{hs}}$ , we examine two limiting cases with  $\Gamma_j\beta_j = 1$  and  $\beta_{\text{hs}} = 0.01$  being a High- $n$  case, and that with  $\Gamma_j\beta_j = 30$  and  $\beta_{\text{hs}} = 0.06$  being a Low- $n$  case. For the High- $n$  case,  $n_{-}$  is about two orders of magnitude larger than that of the Low- $n$  case.

In Fig. 4, we show the allowed region of  $n_{-}$  and  $n_p$  for the High- $n$  case. First of all, we find that  $n_{-} > n_p$  always holds and this satisfies  $\eta \sim 10^{-2}$  at  $P = P_{\text{max}}$ .

This implies that positron mixture is inevitable. In other words,  $P_{1,\min}$  is much larger than  $P_{\max}$  obtained by the Cygnus A cocoon calorimetry. (If we are force to make  $P_{1,\min}$  smaller, then  $\gamma_{\min}$  becomes larger and such a case coincides with (b).) The allowed regions of  $n_-$  and  $n_p$  are further divided by two regions. The pair of light-gray regions show the one in which  $P_{\pm} > P_p$  is satisfied. On the contrary, the pair of dark-gray regions display the one in which  $P_{\pm} < P_p$  holds. Interestingly, we find that the regions of  $P_p < P_{\pm}$  and  $P_p > P_{\pm}$  are both wide in the range of allowed  $P$ . Only in the range of  $P \sim (3 - 6) \times 10^{-10}$  ergcm $^{-3}$ , the pair dominance  $P_p < P_{\pm}$  alone is permitted in the High- $n$  case.

Fig. 5 displays the result for the Low- $n$  case. Similar to the High- $n$  case,  $n_- > n_p$  always holds and they satisfy  $\eta \sim 10^{-1}$  at  $P = P_{\max}$ . Due to the decrease in  $n_{-, \min}$ , the number densities in allowed regions are about two orders of magnitude smaller than that for the High- $n$  case shown in Fig. 4. Correspondingly,  $P_{0,\min}$ ,  $P_{\text{eq},\min}$ , and  $P_{1,\min}$  decrease. Since  $P_{\text{eq},\max} < P_{\max}$  is still satisfied, both of the regions with  $P_p < P_{\pm}$  and that with  $P_p > P_{\pm}$  are allowed in this case. In other words, the Low- $n$  case also draws the same conclusion with the High- $n$  case qualitatively. Quantitatively, the upper limit of  $n_p$  becomes larger when  $n_{-, \min}$  becomes smaller and correspondingly the maximum  $\eta$  achieved at  $P_{\max}$  becomes larger by a factor of  $\sim 10$  than that for the High- $n$  case.

In summarizing case (a), we find that  $\eta < 1$  always holds in the allowed range of  $P$ . In other words, this indicates the existence of  $e^{\pm}$  pairs in the cocoon. We find that (i)  $e^{\pm}$  pair is dominant in terms of number density, and (ii) both the ‘‘pair-supported cocoon (i.e.,  $P_{\pm} > P_p$ )’’ and the ‘‘proton-supported one (i.e.,  $P_{\pm} < P_p$ )’’ are allowed. The pair-supported cocoon is different from the previously suggested one in which protons are dynamically dominated (e.g., De Young 2006).

#### 6.2.2. Case (b)

For Cygnus A, we face a difficulty of realizing one-temperature plasma. First, let us consider the case of same  $n_{-, \min}$  as in Figs. 4 and 5. Then all of these thermal electrons should be heated up to  $kT_{\pm} \sim 10^4 m_e c^2$  and injected into the lobes in the case (b). In the radio lobes, Yaji et al. (2010) evaluates the number density of non-thermal electrons as  $\sim 10^{-7}$  cm $^{-3}$  at  $\gamma_- \sim 10^4$ . So, if we allow the existence of thermal plasma with the same  $n_{-, \min}$  in Figs. 4 and 5 but with  $kT_{\pm} = kT_p \sim 10^4 m_e c^2$ , a big thermal bump at  $\sim 10^9$  Hz should appear. However there is no such bump in the observed spectra of the radio lobes. Therefore, we can exclude the case of the same  $n_{-, \min}$  with  $kT_{\pm} = kT_p \sim 10^4 m_e c^2$ .

Next, we consider smaller  $n_{-, \min}$ . Using the relation  $n_{-, \min} \propto \gamma_{\text{hs}, \min}^{-1}$  in Eq. (19), the increase in  $\gamma_{\text{hs}, \min}$  leads to the decrease in  $n_{-, \min}$  in Figs. 4 and 5; basically,  $\gamma_{\text{hs}, \min} \sim 10^4$  is required at the hot spot (e.g., Harris et al. 2000; Hardcastle, Birkinshaw, and Worrall 2001; Blundell et al. 2006; Godfrey et al. 2009). However, in the case of Cygnus A, the model spectra of the hot spots with  $\gamma_{\text{hs}, \min} \geq 2000$  conflict with the observed ones (KT04). Therefore, case (b) is not likely for Cygnus A.

#### 6.2.3. Case (c)

Let us consider the case of dominant non-thermal pressures and a separate acceleration of electrons and protons with a steep power law spectrum. This is almost identical to (a). A slight difference between this case and (a) is the evaluation of  $n_{-, \min}$ . Since non-thermal pairs are dominated in this case, the allowed region would be limited around  $n_- \approx n_{-, \min}$  in Figs. 4 and 5.

#### 6.2.4. Case (d)

Let us consider case (d). The factor  $A_{\pm} = (\gamma_{\pm, \text{crit}}/\gamma_{\pm, \min})^{-s+2}$  in Eq. (14) is the only element to change the result from (a). Since  $\gamma_{\text{crit}, \pm} \sim m_p/m_e$  is suggested by Stawarz et al. (2007), we can estimate  $A_{\pm}$  as  $A_{\pm} \approx 14(\Gamma_j/10)^{0.5}$  for  $s_{e,1} = 1.5$ . Therefore, a difference between this case and (a) is the larger  $P_{\pm}$  by a factor of  $A_{\pm}$ . Although the spectral break may be suggested from radio observations for case (d),  $n_-^{\text{NT}}$  is dominated by electrons at a break energy  $\gamma_{\text{crit}, \pm} m_e c^2$  and proton energies are not entirely transported to electrons. Therefore, results of (d) are expected to be intermediate between cases (a) and (b).

## 7. SUMMARY AND DISCUSSIONS

In this work, we propose a new method for testing plasma composition of AGN jets by using the cocoon dynamics. In particular, we properly evaluate partial pressures of protons and  $e^{\pm}$  pairs. The point of the method is that  $n_p$  and  $P_p$  can be constrained by considering the global conservations of kinetic energy, mass, and momentum of shocked plasma in the cocoon. Regarding particle distribution functions in the cocoon, it is hard to determine them uniquely because of sparseness of observational data. Therefore, we examine four typical cases in this work. Cases (a), (b), (c) and (d) respectively present two-temperature thermal plasma, one-temperature thermal plasma, non-thermal plasma with their spectral indices harder than two, and non-thermal plasma with a broken power-law electron spectrum.

The three significant advantages of the present work compared with previous work are summarized as follows;

1.  $P$  estimate is based on global cocoon dynamics. Since it is beaming-independent calorimetry of the true amount of energy released by the jet, the estimate of  $P$  from cocoon dynamics has fewer uncertainties compared with blazar studies.
2. We focus on powerful FR II sources. Relativistic hydrodynamic simulations tell us that FR II sources have less entrainment phenomena than FR I sources. Therefore, FR IIs are better for testing genuine plasma composition of AGN jets.
3. We properly deal with the partial pressure of thermal electrons/positrons  $P_{\pm}^{\text{T}}$ . Although  $P_{\pm}^{\text{T}}$  is a critically important finite quantity, most prior efforts assume  $P_{\pm}^{\text{T}} = 0$  merely for simplicity.

Applying the method to the best studied FR II source Cygnus A, we draw the following conclusions which primarily indicate the existence of numerous  $e^{\pm}$  pairs in the cocoon of Cygnus A.

- Cases (a), (c) and (d), in which the average energy of electrons and positrons is significantly lower than

that of protons ( $\eta < 10^{-1}$  for Low- $n$  case;  $\eta < 10^{-2}$  for High- $n$  case), are allowed without violating the observational constraints. The results in (a) and (c) are almost the same, except that the lowest energy electrons are thermal ones and non-thermal ones for (a) and (c), respectively. Cases (a) and (d) also show similar results but for a larger  $P_{\pm}$  in (d) by a factor of  $\sim 14$  than the one in (a).

- We can rule out case (b) in which electrons and positrons are heated up to the proton temperature of  $\sim 10^4 m_p c^2$ . Because there is no thermal bump due to the hot thermal plasma.
- For (a), (c) and (d), we find that the number density of  $e^{\pm}$  is larger than  $n_p$  in any allowed  $P$  and the obtained  $n_+$  is always more than 10 times larger than  $n_p$ . We conclude that pure  $e/p$  plasma is excluded and  $e^{\pm}$ -proton mixture composition is achieved in the Cygnus A jet. Therefore, further studies on the  $e^{\pm}$  pair loading problem extending previous ones (e. g., Blandford & Levinson 1995; Li & Liang 1996; Thompson 1997; Beloborodov 1999; Yamasaki, Takahara & Kusunose 1999) will be more important and the study of its bulk acceleration of  $e^{\pm}$  outflow (Iwamoto and Takahara 2002, 2004; Asano and Takahara 2007, 2009) will also be

highly motivated.

- We find that both  $e/p$  plasma and  $e^{\pm}$  pair pressure supported scenarios are permitted within the limit of current observational constraints. We quantitatively show the allowed regions of  $P_p > P_{\pm}$  and  $P_p < P_{\pm}$  by our new method (see Figs. 4 and 5).

Lastly we add a brief comment on  $P_p^{\text{NT}}$ . Recently Atoyan and Dermer (2008) has suggested the possibility of a secondary emission induced by high-energy protons at Cygnus A. The luminosity of the secondary emission depends on  $P_p^{\text{NT}}$ . If the emission is detected in the future, it will provide us a new direct constraint on  $P_p^{\text{NT}}$ . It could also give us a new constraint on cosmic-ray propagations influenced by the galactic magnetic field (Dermer et al. 2009).

#### ACKNOWLEDGMENTS

We thank the referee for useful suggestions for major improvement of the original manuscript. We also thank H. Ito for helpful discussions. This work is supported in part by Ministry of Education, Culture, Sports, Science, and Technology (MEXT) Research Activity Start-up 2284007 (NK).

#### REFERENCES

- Achterberg, A., Gallant, Y. A., Kirk, J. G., & Guthmann, A. W. 2001, *MNRAS*, 328, 393
- Amato, E., & Arons, J. 2006, *ApJ*, 653, 325
- Arnaud, K. A., Fabian, A. C., Eales, S. A., Jones, C., & Forman, W., 1984, *MNRAS*, 211, 981
- Asano, K., & Takahara, F., 2007, *ApJ*, 655, 762
- Asano, K., & Takahara, F., 2009, *ApJ*, 690, L81
- Atoyan, A., & Dermer, C. D., 2008, *ApJ*, 687, L75
- Bach, U., Krichbaum, T. P., Alef, W., Witzel, A., & Zensus, J. A., 2002, *Proceedings of the 6th European VLBI Network Symposium*, eds.: E. Ros, R. W. Porcas, A. P. Lobanov, and J. A. Zensus, p. 155
- Bach, U., Kadler, M., Krichbaum, T. P., Middelberg, E., Alef, W., Witzel, A., & Zensus, J. A., 2003, *Proceedings of the Second ENIGMA Meeting*, eds.: C. M. Raiteri and M. Villata, p. 216
- Bednarz, J., & Ostrowski, M. 1998, *Physical Review Letters*, 80, 3911
- Begelman, M. C., Blandford, R. D., & Rees, M. J. 1984, *Rev. Mod. Phys.*, 56, 255
- Begelman, M. C., & Cioffi, D. F., 1989, *ApJ*, 345, L21
- Beloborodov, A. M., 1999, *MNRAS*, 305, 181
- Bicknell, G. V., 1984, *ApJ*, 286, 68
- Birzan, L., McNamara, B. R., Nulsen, P. E. J., Carilli, C. L., & Wise, M. W., 2008, *ApJ*, 686, 859
- Blandford, R. D., & Znajek, R. L. 1977, *MNRAS*, 179, 433
- Blandford, R. D., & Levinson, A., 1995, *ApJ*, 441, 79
- Blundell, K. M., Fabian, A. C., Crawford, C. S., Erlund, M. C., & Celotti, A., 2006, *ApJ*, 644, L13
- Carilli, C. L., Perley, R. A., & Dreher, J. H. 1988, *ApJ*, 334, L73
- Carilli, C. L., Perley, R. A., Dreher, J. W., & Leahy, J. P. 1991, *ApJ*, 383, 554
- Carilli, C. L., & Barthel, P. D., 1996, *A&ARv*, 7, 1
- Carilli, C. L., Perley, R., Harris, D. E., & Barthel, P. D., 1998, *Physics of Plasmas*, 5, 1981
- Cavagnolo, K. W., McNamara, B. R., Nulsen, P. E. J., Carilli, C. L., Jones, C., & Birzan, L., 2010, *ApJ*, 720, 1066
- Croston, J. H., Hardcastle, M. J., Harris, D. E., Belsole, E., Birkinshaw, M., & Worrall, D. M., 2005, *ApJ*, 626, 733
- Dermer, C. D., Razaque, S., Finke, J. D., & Atoyan, A. 2009, *New Journal of Physics*, 11, 065016
- De Young, D. S., 1993, *ApJ*, 405, L13
- De Young, D. S., 2006, *ApJ*, 648, 200
- Dreher J. W., Carilli C. L., Perley R. A., 1987, *ApJ*, 316, 611
- Dunn, R. J. H., Fabian, A. C., & Taylor, G. B., 2005, *MNRAS*, 364, 1343
- Fabian, A. C., Celotti, A., Blundell, K. M., Kassim, N. E., & Perley, R. A., 2002, *MNRAS*, 331, 369
- Garrington, S. T., & Conway, R. G. 1991, *MNRAS*, 250, 198
- Georganopoulos, M., Kazanas, D., Perlman, E., & Stecker, F. W., 2005, *ApJ*, 625, 656
- Ghisellini, G., & Tavecchio, F. 2010, *MNRAS*, 409, L79
- Godfrey, L. E. H., et al., 2009, *ApJ*, 695, 707
- Hardcastle, M. J., Birkinshaw, M., & Worrall, D. M., 2001, *MNRAS*, 323, L17
- Hardcastle, M. J., & Croston, J. H., 2010, *MNRAS*, 404, 2018
- Harris, D. E., & Krawczynski, H., 2006, *ARA&A*, 44, 463
- Harris, D. E., et al., 2000, *ApJ*, 530, L81
- Hirotoni, K., Iguchi, S., Kimura, M., & Wajima, K., 1999, *PASJ*, 51, 263
- Hirotoni, K., Iguchi, S., Kimura, M., & Wajima, K., 2000, *ApJ*, 545, 100
- Hirotoni, K., 2005, *ApJ*, 619, 73
- Homan, D. C., Lister, M. L., Aller, H. D., Aller, M. F., & Wardle, J. F. C., 2009, *ApJ*, 696, 328
- Hoshino, M., Arons, J., Gallant, Y. A., & Langdon, A. B. 1992, *ApJ*, 390, 454
- Huang, L., & Shcherbakov, R. V. 2011, *MNRAS*, 416, 2574
- Ichimaru, S. 1973, *Basic principles of plasma physics, a statistical approach.*, by Ichimaru, S.. Reading, MA (USA): Benjamin, 324 p.,
- Isobe, N., Tashiro, M., Makishima, K., Iyomoto, N., Suzuki, M., Murakami, M. M., Mori, M., & Abe, K., 2002, *ApJ*, 580, L111
- Isobe, N., Makishima, K., Tashiro, M., & Hong, S., 2005, *ApJ*, 632, 781
- Ito, H., Kino, M., Kawakatu, N., Isobe, N., & Yamada, S., 2008, *ApJ*, 685, 828 (I08)
- Iwamoto, S., & Takahara, F., 2002, *ApJ*, 565, 163
- Iwamoto, S., & Takahara, F. 2004, *ApJ*, 601, 78
- Kataoka, J., et al., 2008, *ApJ*, 672, 787
- Kawakatu, N., & Kino, M., 2006, *MNRAS*, 370, 1513
- Kellermann, K. I., & Pauliny-Toth, I. I. K. 1981, *ARA&A*, 19, 373
- Kellermann, K. I., et al., 2004, *ApJ*, 609, 539
- Kino, M., Takahara, F., 2004, *MNRAS*, 349, 336 (KT04)
- Kino, M., & Kawakatu, N., 2005, *MNRAS*, 364, 659



- Kino, M., Kawakatu, N., & Ito, H., 2007, *MNRAS*, 376, 1630
- Kino, M., & Takahara, F., 2008, *MNRAS*, 383, 713
- Kirk, J. G., Guthmann, A. W., Gallant, Y. A., & Achterberg, A. 2000, *ApJ*, 542, 235
- Komissarov, S. S., Barkov, M. V., Vlahakis, N., Königl, A. 2007, *MNRAS*, 380, 51
- Krichbaum, T. P., Alef, W., Witzel, A., Zensus, J. A., Booth, R. S., Greve, A., & Rogers, A. E. E., 1998, *A&A*, 329, 873
- Lazio, T. J. W., Cohen, A. S., Kassim, N. E., Perley, R. A., Erickson, W. C., Carilli, C. L., & Crane, P. C., 2006, *ApJ*, 642, L33
- Li, H., & Liang, E. P., 1996, *ApJ*, 458, 514
- Lister, M. L., Tingay, S. J., Murphy, D. W., Piner, B. G., Jones, D. L., & Preston, R. A., 2001, *ApJ*, 554, 948
- Lister, M. L., et al., 2009, *AJ*, 137, 3718
- Machalski J., Jamroz M., Konar C., 2010, *A&A*, 510, A84
- Melrose, D. B. 1997, *Journal of Plasma Physics*, 58, 735
- Miley, G. 1980, *ARA&A*, 18, 165
- Mizuta, A., Yamada, S., & Takabe, H., 2004, *ApJ*, 606, 804
- McKinney, J. C., 2006, *MNRAS*, 368, 1561
- McKinney, J. C., Tchekhovskoy, A., & Blandford, R. D. 2012, [arXiv:1201.4163](https://arxiv.org/abs/1201.4163)
- Mehta, K. T., Georganopoulos, M., Perlman, E. S., Padgett, C. A., & Chartas, G., 2009, *ApJ*, 690, 1706
- Perley, R. A., Dreher, J. W., & Cowan, J. J., 1984, *ApJ*, 285, L35
- Perlman, E. S., Georganopoulos, M., May, E. M., & Kazanas, D. 2010, *ApJ*, 708, 1
- Perucho, M., & Martí J. M., 2007, *MNRAS*, 382, 526
- Quataert, E., & Gruzinov, A. 2000, *ApJ*, 545, 842
- Rachen, J. P., & Biermann, P. L. 1993, *A&A*, 272, 161
- Rafferty, D. A., McNamara, B. R., Nulsen, P. E. J., & Wise, M. W., 2006, *ApJ*, 652, 216
- Rawlings, S., & Saunders, R., 1991, *Nature*, 349, 138
- Reynolds, C. S., Fabian, A. C., Celotti, A., & Rees, M. J., 1996, *MNRAS*, 283, 873
- Rossi, P., Mignone, A., Bodo, G., Massaglia, S., & Ferrari, A., 2008, *A&A*, 488, 795
- Ruszkowski, M., & Begelman, M. C., 2002, *ApJ*, 573, 485
- Scheck, L., Aloy, M. A., Martí, J. M., Gómez, J. L., & Müller, E., 2002, *MNRAS*, 331, 615
- Scheuer, P. A. G., 1995, *MNRAS*, 277, 331
- Sikora, M., & Madejski, G., 2000, *ApJ*, 534, 109
- Sironi, L., & Spitkovsky, A., 2011, *ApJ*, 726, 75
- Spitkovsky, A., 2008, *ApJ*, 682, L5
- Stawarz, L., Cheung, C. C., Harris, D. E., & Ostrowski, M., 2007, *ApJ*, 662, 213
- Steenbrugge, K. C., Blundell, K. M., & Duffy, P., 2008, *MNRAS*, 388, 1465
- Steenbrugge, K. C., Heywood, I., & Blundell, K. M., 2010, *MNRAS*, 401, 67
- Smith, D. A., Wilson, A. S., Arnaud, K. A., Terashima, Y., & Young, A. J., 2002, *ApJ*, 565, 195
- Svensson, R., 1982, *ApJ*, 258, 335
- Takahara, F. 1990, *Progress of Theoretical Physics*, 83, 1071
- Thompson, C., 1997, in Ostrowski, M., Sikora, M., Madejski, G., Begelman, M., eds., *Proc. Int. Conf., Relativistic Jets in AGNs*. Cracow, p. 63
- Tashiro, M., et al., 1998, *ApJ*, 499, 713
- Tashiro, M. S., Isobe, N., Seta, H., Matsuta, K., & Yaji, Y., 2009, *PASJ*, 61, 327
- Uchiyama, Y., Urry, C. M., Van Duyne, J., Cheung, C. C., Sambruna, R. M., Takahashi, T., Tavecchio, F., & Maraschi, L., 2005, *ApJ*, 631, L113
- Wardle, J. F. C., Homan, D. C., Ojha, R., & Roberts, D. H., 1998, *Nature*, 395, 457
- Watanabe, S., et al. 2009, *ApJ*, 694, 294
- Wilson, A. S., Young, A. J., & Shopbell, P. L., 2000, *ApJ*, 544, L27
- Wilson, A. S., Smith, D. A., & Young, A. J., 2006, *ApJ*, 644, L9
- Yaji, Y., Tashiro, M., Isobe, N., Kino, M., Asada, K., Nagai, H., Koyama, S., & Kusunose, M., 2010, *ApJ*, 714, 37
- Yamasaki, T., Takahara, F., & Kusunose, M., 1999, *ApJ*, 523, L21

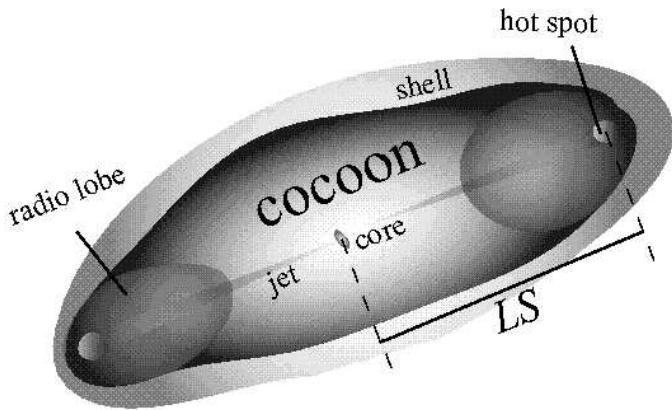


FIG. 1.— A cartoon of a powerful FR II radio galaxy. A pair of jets is ejected from the core and they are decelerated via strong shocks. The shocks are identified as the hot spots and the remnant of decelerated jets envelopes the overall jet system and this is identified as a cocoon. Part of cocoon is normally observed as radio lobes. The cocoon head and the hot spots advance at a speed  $v_{\text{hs}}$ . Swept-up ambient matter becomes a shell and surrounds the cocoon. The projected linear size is denoted as  $LS$  in this work.

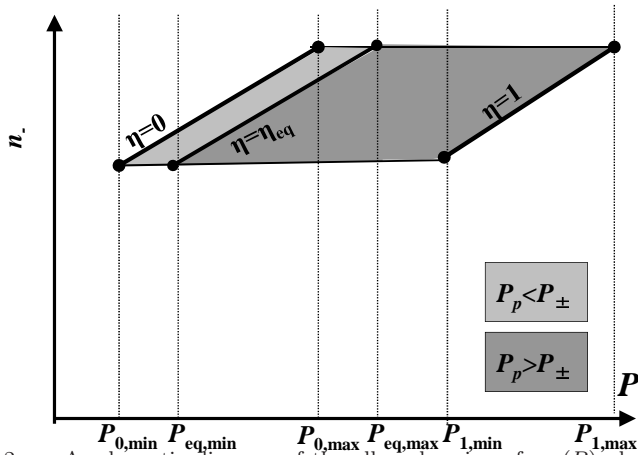


FIG. 2.— A schematic diagram of the allowed region of  $n_-(P)$  plotted versus the cocoon pressure  $P$  for given  $\Gamma_j$ . They are limited by  $n_{-,min} \leq n_- \leq n_{-,max}$  and  $0 \leq \eta \leq 1$ . The region of  $e^\pm$ -supported cocoon ( $P_\pm > P_p$ ) is colored in light gray while the region of proton-supported cocoon ( $P_p > P_\pm$ ) is colored in dark gray.

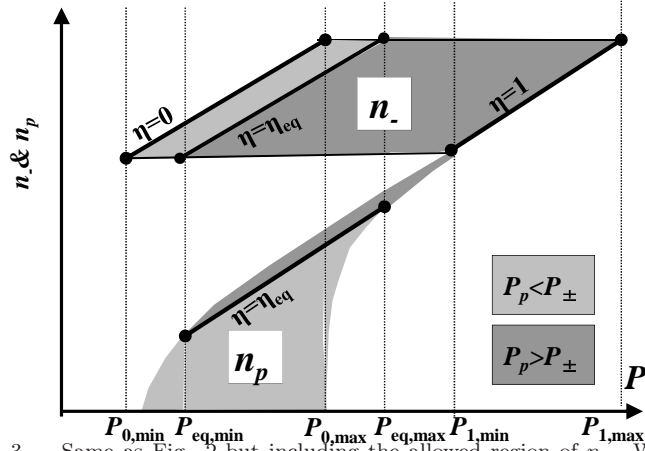


FIG. 3.— Same as Fig. 2 but including the allowed region of  $n_p$ . When  $\eta = 1$ ,  $n_- = n_p$  holds by definition. When  $\eta < 1$ , positron mixture is required by the charge neutrality condition of  $n_- = n_p + n_+$ . The plane is divided into 5 regions by characteristic pressures. The actual allowed region is further limited within  $P_{\min} \leq P \leq P_{\max}$  by the consideration of cocoon calorimetry.

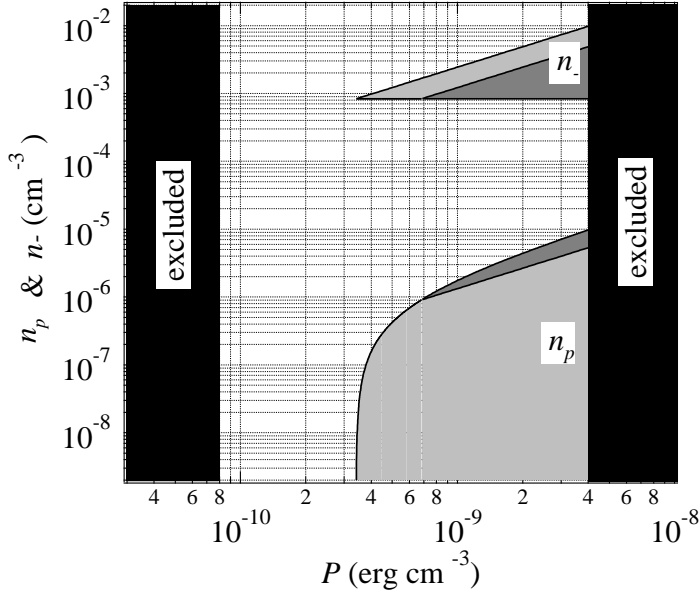


FIG. 4.— Allowed regions of  $n_-$  and  $n_p$  for Cygnus A with  $\Gamma_j \beta_j = 1$  and  $\beta_{\text{hs}} = 0.01$  (we call this the High- $n$  case). The region within  $8 \times 10^{-11} \text{ erg cm}^{-3} \leq P \leq 4 \times 10^{-9} \text{ erg cm}^{-3}$  shown here is the one allowed for Cygnus A. As explained in Fig. 3, the region in which  $P_{\pm} > P_p$  holds is colored in light gray while the region where  $P_{\pm} < P_p$  is satisfied is colored in dark gray. It is found that  $e^{\pm}$  pairs always dominate in terms of number density but either “pair-supported cocoon (i.e.,  $P_{\pm} > P_p$ )” or “proton-supported one (i.e.,  $P_{\pm} < P_p$ )” is possible.

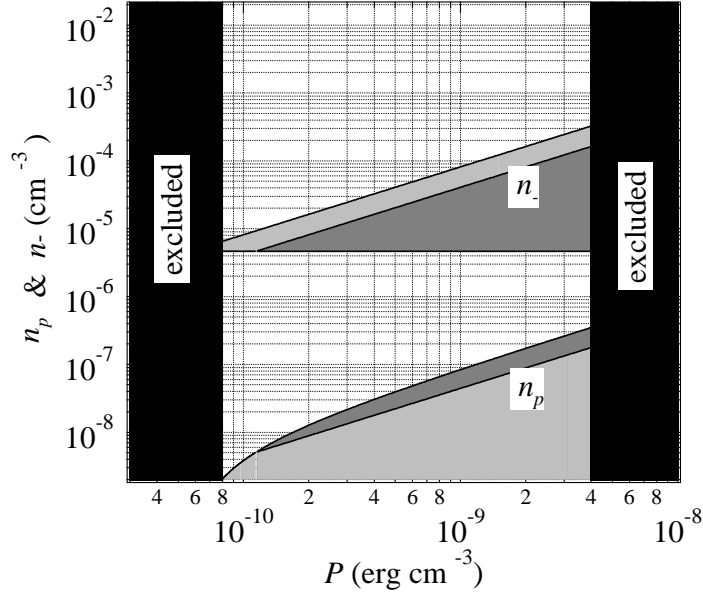


FIG. 5.— Same as Fig. 5 but with  $\Gamma_j = 30$  and  $\beta_{hs} = 0.06$  (we call this the Low- $n$  case). Although the allowed regions of  $n_-$  and  $n_p$  are about two orders of magnitude smaller than the ones in Fig. 4 (High- $n$  case), the Low- $n$  case also draws the same conclusion as the High- $n$  case.